RSC Advances

ROYAL SOCIETY OF CHEMISTRY

PAPER

View Article Online
View Journal | View Issue

Cite this: *RSC Adv.*, 2026, **16**, 18697

Sensitive and eco-friendly extraction of antifungal drugs from artificial urine and saliva samples using MSPE coupled with HPLC-DAD

Amina Ben Ayed, [a] Songül Ulusoy, *[b] Halil İbrahim Ulusoy, *[c] Ümmügülsüm Polat[c] and Hamadi Khemakhem[a]

The analysis of drug molecules in biological samples is a challenge for method development studies. The existence of matrix components and trace concentrations of target molecules in the samples make this analysis more difficult. Sample pre-treatment procedures, such as solid-phase micro extraction (SPME), facilitate and make this analysis possible using conventional analytical techniques such as HPLC. A newly synthesized trimesic acid (TMA)-modified magnetic adsorbent, Fe_3O_4@SiO_2–TMA, effectively retained drug molecules, enabling the successful determination of bifonazole (BFZ) and itraconazole (ITZ) residues in model solutions, including artificial saliva and urine samples. The characterization of the new adsorbent was performed by scanning electron microscopy (SEM), Fourier transform infrared (FTIR) spectroscopy, X-ray diffraction (XRD) and Raman spectroscopy. The linear ranges for both target molecules were 15.00–1000.00 ng mL^{-1} (R^2 > 0.9954), with a limit of detection lower than 5.00 ng mL^{-1}. The accuracy and repeatability of the proposed method were determined as recovery (*R*%) and relative standard deviation (RSD%) using spiked samples. This study presented the synthesis and characterization of Fe_3O_4@SiO_2–TMA, a new magnetic adsorbent, for the accurate and precise analysis of BFZ and ITZ, known as antifungal molecules, in biological samples. A straightforward and efficient determination of the target compounds was achieved using a magnetic solid-phase extraction (MSPE) procedure coupled with a high-performance liquid chromatography system equipped with a diode array detector (HPLC-DAD). The greenness and practical applicability of the method were assessed using BAGI and MoGAPI tools, with scores of 65 and 76, respectively. The developed method was successfully applied to real biological samples, yielding recovery values between 94.7% and 107.5%. These results demonstrate that the proposed approach is sensitive, reliable, and environmentally sustainable for routine antifungal drug analysis.

Received 23rd December 2025
Accepted 23rd March 2026

DOI: 10.1039/d5ra09942k

rsc.li/rsc-advances

1. Introduction

Over the last few decades, fungal infections have been a serious public health concern worldwide. This rise is closely associated with the increasing number of immunocompromised individuals, which has emerged because of modern medical practices, including the extensive use of intensive chemotherapy and immunosuppressive agents.[1] Fungal infections can affect various parts of the body, including the mouth, throat, vagina, fingers, nails, trachea, lungs, skin, and gastrointestinal tract. The management of bacterial and fungal infections typically involves the use of medical antifungal agents in both human and veterinary medicine. Currently, four major classes of antifungal drugs, azoles, echinocandins, polyenes, and pyrimidine analogs, are administered through oral, topical, or intravenous routes for the treatment of such infections.[2] Azoles are a heterogeneous group of antifungal drugs. Moreover, these agents are extensively employed as first-line treatments for both systemic and topical fungal infections across the world owing to their broad-spectrum efficacy and relatively low cost.[3] Azoles can be classified into two groups: those with two nitrogen atoms in the azole ring, called imidazoles, including clotrimazole, econazole, ketoconazole, and bifonazole, and those with three nitrogen atoms in the azole ring, called triazoles, such as fluconazole, itraconazole, posaconazole, voriconazole and isavuconazole.[4] Furthermore, these compounds are recognized for their broad and potent antifungal activities against numerous pathogenic fungi. Itraconazole (ITZ), a member of the triazole class, is commonly prescribed for the treatment of fungal infections, such as aspergillosis and histoplasmosis, and it is generally well-tolerated by patients.[5,6] Bifonazole (BFZ),

[a]*Laboratory of Multifunctional Materials and Applications (LaMMA), Faculty of Sciences of Sfax, University of Sfax, BP 1171, 3000 Sfax, Tunisia*
[b]*Department of Pharmacy, Vocational School of Health Service, Sivas Cumhuriyet University, Sivas, Türkiye. E-mail: sonulusoy@yahoo.com*
[c]*Department of Analytical Chemistry, Faculty of Pharmacy, Sivas Cumhuriyet University, Sivas, Türkiye. E-mail: hiulusoy@yahoo.com*

a relatively new azole derivative, exhibits strong antifungal effects against dermatophytes, yeasts, and molds.[7] In clinical practice, BFZ-based topical formulations are widely utilized for managing toenail onychomycosis, tinea pedis, and yeast-related infections. Nonetheless, its antifungal potential against agricultural pathogens, particularly *Penicillium expansum*, has not been clearly defined and remains poorly characterized. ITZ is typically available in tablet and capsule dosage forms, while BFZ is mainly prepared as creams and powders.[7]

The widespread application of antifungal agents, particularly azole-based compounds, has led to their increased release into the environment, resulting in elevated levels of these substances and their residues. Once introduced into the environment, antifungal drugs tend to partition among various environmental compartments.[8] The occurrence of such residues poses potential ecotoxicological threats to non-target organisms. Environmentally relevant concentrations of the azole antifungals have been linked to endocrine-disrupting effects, alterations in microbial community dynamics, the modulation of gene expression, the inhibition of larval growth and development, and the heightening of chemical sensitivity. Moreover, the extensive and repetitive use of these agents, especially azoles, has contributed to the emergence of antifungal resistance both in clinical settings and in natural environments, thereby limiting available therapeutic options for fungal infections.[9] Owing to their persistence, possible ecotoxicity, and role in fostering drug resistance, the environmental presence of antifungal agents has become a significant concern. As a result, exploring the distribution and environmental occurrence of azole antifungals in fungal isolates has emerged as a rapidly growing research field. Considering that both BFZ and ITZ belong to the azole class, their sensitive and selective detection in contaminated environments is of great importance.

In recent years, various analytical techniques have been developed for the detection of azole antifungals, such as high-performance liquid chromatography (HPLC) coupled with ultraviolet (UV) detection,[10] gas chromatography (GC),[11] enzyme-linked immunosorbent assay (ELISA)[12] liquid chromatography-mass spectrometry (LC-MS),[13] and thin-layer chromatography (TLC).[14] Although these methods generally provide reliable results, they still suffer from several drawbacks, including lengthy analytical procedures, limited selectivity, and high operational costs—particularly when analyzing complex matrices or trace-level analytes. Hence, the development of simple, highly selective, and sensitive sample pretreatment strategies is of great importance.

Azole antifungal drugs are frequently detected in environmental and biological matrices due to their widespread clinical and veterinary use. Reported studies have indicated that triazole derivatives, including itraconazole, may occur in wastewater, surface waters, and biological fluids at trace levels ranging from ng L^{-1} to μg L^{-1}. Similarly, bifonazole residues have been monitored in pharmaceutical formulations and biological samples following topical or systemic exposure. The persistence of these compounds and their potential ecotoxicological effects, even at low concentrations, highlight the necessity for developing highly sensitive, selective, and reliable analytical methodologies for their determination in complex matrices. At present, numerous advanced pretreatment techniques have been introduced, including solid-phase extraction (SPE),[15] solid-phase microextraction (SPME),[16] magnetic solid-phase extraction (MSPE),[17] dispersive solid-phase extraction (dSPE),[18] and dispersive liquid–liquid microextraction (DLLME).[19] Among these, MSPE—an evolution of conventional SPE—enables the rapid and efficient separation of magnetic adsorbent particles from the liquid phase using an external magnetic field.[21] During the MSPE process, magnetic particles are homogeneously dispersed in the sample solution through agitation, ultrasonication, or vortexing, which significantly reduces mass-transfer equilibrium time.[20] Consequently, MSPE has gained recognition as a powerful and efficient preconcentration and separation technique that simplifies sample preparation while enhancing extraction efficiency.

As with other extraction techniques, the choice of magnetic adsorbent plays a critical role in the efficiency of the MSPE process. In recent years, various materials—such as carbon nanotubes (CNTs),[19] graphene and graphene oxide (G/GO),[21] and metal–organic frameworks (MOFs)[22]—have been investigated as magnetic adsorbents. Among these, iron oxide (Fe_3O_4)-based magnetic particles have attracted significant attention due to their tunable structure, uniform porosity, large surface area, abundance of active functional groups, and versatile modification potential.[23]

Magnetic core–porous shell systems offer effective separation and isolation capabilities, as the porous shell adsorbs metal ions while the magnetic core enables the easy retrieval of particles from the solution. Trimesic acid (TMA), an organic molecule containing multiple carboxylic groups, is particularly useful for such systems because of its ability to form coordination bonds in metal–organic frameworks and coordination polymers,[24,25] as well as its strong affinity for toxic metals and organic contaminants.[26,27] TMA can function as both a hydrogen donor and acceptor through the formation of diverse resonance structures. Owing to its structural symmetry and multiple acidic functional sites, TMA can be immobilized on the surface of magnetic nanoparticles (MNPs) to enhance their selectivity and stability. To maintain the chemical integrity and functionality of the core–shell structure, a silica (SiO_2) interlayer between Fe_3O_4 and TMA is essential. The SiO_2 coating not only improves the chemical and thermal stability of the magnetic core but also enhances its dispersibility and resistance to harsh acidic environments.[28]

The aim of this study was to create Fe_3O_4@SiO_2–TMA magnetic nanoparticles *via* a green synthesis approach and then utilize them to adsorb bifonazole (BFZ) and itraconazole (ITZ) in biological samples (artificial saliva and urine) before HPLC-DAD analysis. To improve efficiency, the extraction parameters, such as extraction time, sample volume, pH, and elution solvent, were systematically optimized. The synthesized adsorbent exhibited an ideal extraction performance by showing high selectivity and sensitivity, highlighting its suitability as an efficient material for MSPE applications. Furthermore, the proposed method was compatible with green

chemistry principles by minimizing resource consumption and reducing operational costs, thereby offering an environmentally sustainable and economically viable analytical approach.

2. Materials and methods

2.1 Chemicals and materials

Bifonazole (BFZ, purity ≥ 99%) and itraconazole (ITZ, purity ≥ 99%) standard reference materials were obtained from Sigma, USA. All other chemicals and solvents were of analytical or HPLC grade. All chemicals used in this study had a minimum purity of 99.5%. Ammonium iron(II) sulfate hexahydrate ($Fe(NH_4)_2(SO_4)_2 \cdot 6H_2O$), iron(III) nitrate nonahydrate ($Fe(NO_3)_3 \cdot 9H_2O$), tetraethoxysilane (TEOS), and trimesic acid (TMA) were obtained from Sigma-Aldrich. Deionized water with a resistivity of 18.2 MΩ cm, produced using a MES Minipure Dest Up purification system, was used throughout all experiments. Chromatographic-grade solvents, including methanol and acetonitrile, were purchased from Sigma (St. Louis, MO, USA) for HPLC analyses.

A series of Britton–Robinson (BR) buffer solutions covering the pH range of 2–10 were prepared from a 0.02 M stock BR solution containing H_3BO_3, H_3PO_4, and acetic acid. The desired pH values were adjusted by the gradual addition of 0.1 M NaOH under continuous monitoring with a calibrated pH meter. Stock solutions of BFZ and ITZ were prepared at a concentration of 1000 μg mL^{-1} using analytical-grade methanol. The stability of BFZ and ITZ in spiked artificial urine and saliva samples was evaluated under storage conditions. Prepared samples were stored at 4 °C and analyzed at predetermined time intervals (0, 24, 48, and 72 h). Recovery values were compared with those of freshly prepared samples to assess potential degradation. No significant loss in analyte concentration was observed, confirming the stability of both antifungal drugs during the storage period.

2.2 Instrumentation

Scanning electron microscopy (SEM) images were acquired using a Philips XL30 scanning electron microscope fitted with an EDAX detector, enabling the detailed structural visualization and analysis of the samples. The homogeneous mixing of various solutions was achieved with a Fisher Scientific digital shaker and a VELP Scientifica F20220176 ZX3 vortex mixer. pH measurements were carried out using a glass-calomel electrode pH meter (Mettler Toledo, Columbus, Ohio, USA). Sample preparation was performed in an ultrasonic water bath (Kudos, China). Prior to chromatographic analysis, all solvents were degassed in an ultrasonic bath for 10 minutes (JP Selecta, Barcelona, Spain) and filtered through 0.45 μm PTFE membrane filters (HNWP, Millipore) under a vacuum using a Buchi pump (Switzerland). The HPLC system consisted of a PDA detector (SPD-M20A), an autosampler (SIL-20Ac), a thermostated column oven (CTO-10AS), and an LC20-AD pump, all from Shimadzu, Tokyo, Japan. Data acquisition and processing were performed using LC Solution software (Shimadzu).

2.3 HPLC-DAD analysis of BFZ and ITZ

The HPLC analysis of BFZ and ITZ was carried out on a C18 column (Luna Omega C18, 250 mm × 4.6 mm, 5.0 μm) under isocratic elution conditions using a mixture of acetonitrile and phosphate buffer at pH 3. The detector wavelengths were set at 256 nm for BFZ and 261 nm for ITZ. The analyses were performed until well-defined peaks corresponding to the target compounds were obtained. Optimized HPLC parameters are summarized in Table 1. As illustrated in Fig. 1, distinct peaks for both bifonazole and itraconazole were observed under the optimized conditions, with peak height and area increasing proportionally with concentration, as expected. Prior to injection, both the samples and mobile phases were degassed ultrasonically for 10 minutes and filtered through a 0.45 μm membrane filter.

2.4 Synthesis of trimesic acid-functionalized magnetic nanoparticles (Fe_3O_4@SiO_2–TMA)

We employed a well-known procedure for the synthesis of Fe_3O_4-based magnetic particles, which was also used in our previous studies.[29–31] For the synthesis of Fe_3O_4 nanoparticles, aqueous solutions of iron(II) ammonium sulfate hexahydrate ($Fe(NH_4)_2(SO_4)_2 \cdot 6H_2O$) and iron(III) nitrate nonahydrate ($Fe(NO_3)_3 \cdot 9H_2O$) were prepared in 0.1 M HCl. Under continuous stirring (600 rpm) and maintained at 60–70 °C, 100 mL of 50%

Table 1 HPLC conditions for the BFZ and ITZ detection

Parameter	Values
HPLC mode	Isocratic
Eluent	70% acetonitrile, 30% pH-3.0 phosphate buffer
DAD, wavelength	256 nm (BFZ), 261 nm (ITZ)
Flow rate	1.0 mL min^{-1}
Run time	14 min
Column	Luna Omega C18, 250 mm × 4.6 mm, 5.0 μm
Column oven temperature	40 °C
Injection volume	10 μL

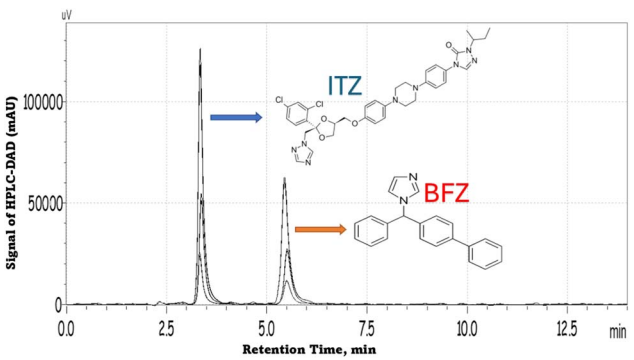

Fig. 1 HPLC chromatogram of the BFZ and ITZ molecules.

(v/v) methanol was gradually introduced into the reaction mixture to facilitate nanoparticle formation. The synthesis was conducted under an inert nitrogen atmosphere to prevent oxidation. Magnetite (Fe_3O_4) nanoparticles were precipitated by the dropwise addition of 30 mL of ammonia solution (25%, w/w) into the vigorously stirred reaction mixture. The resulting Fe_3O_4 particles were magnetically separated, washed repeatedly with a water/methanol mixture (1 : 1, v/v) to remove impurities, and subsequently dried at 60 °C for 6 hours. The final product was stored in a dry tube. To functionalize the magnetite, 2 g of dried Fe_3O_4 nanoparticles were dispersed in a solution containing 100 mL of 50% (v/v) ethanol, 2 mL of concentrated ammonium hydroxide, and 2 mL of tetraethyl orthosilicate (TEOS). This mixture was kept under mechanical stirring (500 rpm) at 25 °C for 6 h to ensure complete silanization. The resulting silica-coated magnetic nanoparticles (Fe_3O_4@SiO_2) were magnetically separated, washed with ethanol to remove unreacted precursors, and dried. Following silanization, the Fe_3O_4@SiO_2 magnetic nanoparticles (MNPs) were functionalized by dispersing them in a reaction mixture containing 30 mg of TMA dissolved in 30 mL of 50% (v/v) methanol. The modification was carried out under continuous mechanical stirring (500 rpm) at 45 ± 5 °C in a nitrogen atmosphere for 6 h to ensure uniform surface conjugation. The resulting Fe_3O_4@SiO_2–TMA composite was then magnetically separated and thoroughly washed with methanol/water (1 : 1, v/v) to remove unreacted TMA. After overnight drying at 40 °C under a vacuum, the product was ground and sieved through a 100-mesh screen to obtain uniformly sized particles (50–100 μm) for subsequent analytical applications.

2.5 The magnetic solid phase extraction (MSPE) process

Under optimum conditions, 50 mg of synthesized Fe_3O_4@SiO_2–TMA MNPs were transferred into tubes of 50 mL. 2 mL of a pH-8 buffer and 10 mL of sample solution, including BFZ and ITZ molecules in the range of 15.00–1000.00 ng mL^{-1}, were added to the tubes, and the final volume was completed to 50 mL with deionized water. Following the adsorption phase, the Falcon tubes were subjected to continuous mixing in an orbital shaker (50 rpm, 40 min) to ensure a homogeneous interaction between the magnetic nanoparticles (MNPs) and target analytes. Post-incubation, the MNP-analyte complexes were magnetically isolated by placing a neodymium magnet at the tube base for 2 min, allowing complete phase separation. The supernatant was carefully decanted using a micropipette or Pasteur pipette while maintaining the tube at a 45° angle to ensure complete liquid removal without disturbing the magnetically immobilized nanoparticle aggregate.

For analyte recovery, the adsorbed species were quantitatively eluted *via* vortex-assisted desorption (400 μL ethanol, 60 s at 100 rpm). The eluate was then filtered through a 0.45 μm PTFE membrane syringe filter to remove particulate residues prior to HPLC-DAD analysis. The filtered extracts were transferred to amber HPLC vials equipped with PTFE-lined caps to prevent solvent evaporation and potential photodegradation.

2.6 Preparation of artificial urine and saliva samples for analytical applications

The developed analytical method was tested with artificial urine, and saliva samples.

Artificial urine was prepared following literature protocols[32–34] to mimic the composition of real urine. The preparation involved dissolving the following components in 500 mL of distilled water: 0.55 g of $CaCl_2 \cdot 2H_2O$, 1.46 g of NaCl, 1.125 g of Na_2SO_4, 0.7 g of KH_2PO_4, 0.8 g of KCl, 0.5 g of NH_4Cl, 12.5 g of urea, and 0.55 g of creatinine. The pH was adjusted to 6.0, and the solution was stored in an amber bottle at 4 °C to prevent degradation. Artificial saliva was prepared by dissolving 4.2 g of sodium hydrogen carbonate, 0.5 g of sodium chloride, 0.2 g of potassium carbonate, and 30 mg of sodium nitrite in water and then diluting the mixture to 1 L. The pH of the solution was adjusted to 5.0 prior to use.

2.7 Preparation of pharmaceutical sample preparations

The developed method was applied to pharmaceutical samples containing antifungal drugs, specifically BFZ and ITZ. For sample preparation, 4.0 g of pomade (ointment) and 0.184 g of capsule powder containing BFZ and ITZ, respectively, were accurately weighed and dissolved in 50 mL of methanol using a volumetric flask. The mixture was then sonicated in a water bath for 10 min to ensure complete dissolution.

Following sonication, 100 mL of water was added, and the solution was agitated for 10 min on an orbital shaker to achieve homogeneity. To complete the preparation, the mixture was diluted with water to 250 mL.

3. Results and discussion

3.1 Characterization of Fe_3O_4 and Fe_3O_4@SiO_2–TMA nanoparticles

3.1.1 Field emission scanning electron microscopy (FE-SEM). Field emission scanning electron microscopy (FE-SEM) was employed to investigate the morphological characteristics of the synthesized Fe_3O_4 and Fe_3O_4@SiO_2–TMA nanoparticles. Images of the synthesized Fe_3O_4 and Fe_3O_4@SiO_2–TMA nanoparticles acquired at 10k and 30k magnification after FE-SEM analysis are shown in Fig. 2. At varying zoom levels, the sub-100 nm structures of the Fe_3O_4 and Fe_3O_4@SiO_2–TMA nanoparticles are visible in images (A) and (B), respectively. Nanoparticles smaller than 100 nm exhibit a broad size distribution and tend to form aggregates of varying dimensions, resulting in a high surface area. Moreover, their intrinsic magnetic properties enable easy separation from the sample matrix. The homogeneity of the magnetite nanoparticles was confirmed by surface morphology analysis. In addition to maintaining this homogeneity, the silica coating (SiO_2–TMA) added functional groups to the structure. FE-SEM images qualitatively demonstrated nanoscale morphology and surface roughness. Quantitative size distribution analysis could not be performed due to instrumental limitations; however, the observed morphology was consistent with those of similar magnetic silica nanocomposites reported in the literature. Consequently, the final

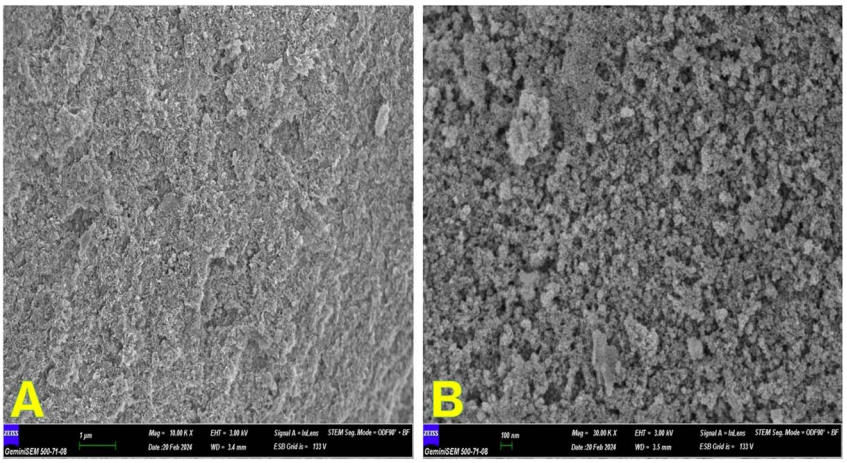

Fig. 2 FE-SEM images of the Fe_3O_4 (A) and Fe_3O_4@SiO_2–TMA (B) magnetic nanoparticles.

composite incorporated the desired surface characteristics of the coating while maintaining the magnetic properties of Fe_3O_4.

3.1.2 Fourier transform infrared (FTIR) spectroscopy. One well-known analytical method for identifying the various functional groups in samples is FTIR. In Fig. 3, the FTIR spectra of various nanoparticles, including Fe_3O_4 and Fe_3O_4@SiO_2–TMA, are displayed. The strong absorption peak at 548 cm^{-1} in both spectra was due to Fe–O stretching vibration.[35] The bands at 1070 and 800 cm^{-1} for coated MNPs were allocated to the stretching and bending vibration of O–Si–O, respectively.[36] Moreover, bands at 1642 and 3400 cm^{-1} were related to O–H stretching and bending. Furthermore, the existence of peaks at 793 and 1064 cm^{-1}, corresponding to the stretching vibrations of Si–O and Si–O–Si, proved the successful coating of SiO_2 on the surface of Fe_3O_4 MNPs. It could be seen that a significant peak at 764 cm^{-1} appeared, which was assigned to the *meta* substitution of the benzene ring of TMA.[37] The FTIR spectrum of TMA was interpreted based on literature-reported characteristic bands, and comparative evaluation was performed accordingly.

3.1.3 Raman spectroscopy. Raman spectroscopy is a potent analytical technique that is utilized to identify molecular vibrations and obtain information about the molecular structure and composition of materials. In addition, Fe_3O_4 and Fe_3O_4@SiO_2–TMA have been characterized by Raman spectroscopy, as can be seen in Fig. 4. In this case, the Raman spectrum peaks of Fe_3O_4 showed the typical intensities located at 190 cm^{-1}, 450 cm^{-1} and 620 cm^{-1} corresponding to $2T_{2g}$ and A_{1g}. However, the band presented at 950 cm^{-1} could be attributed to other ferrite phases.[38]

3.1.4 X-ray diffraction (XRD) analysis. X-ray diffraction (XRD) analysis is widely used to determine the crystallographic structure, phase composition, and other structural properties of materials. XRD analyses were performed for the Fe_3O_4 and Fe_3O_4@SiO_2–TMA nanomaterials synthesized in this study. Characteristic X-ray diffraction spectra were obtained for the Fe_3O_4 nanomaterial and Fe_3O_4@SiO_2–TMA final material, as shown in Fig. 5. First, the XRD diffraction peaks for Fe_3O_4 were obtained at 2-theta angles of 27.31°, 30.88°, 31.64°, 35.42°, 43.39°, 45.59°, 56.61°, 57.47°, 63.21° and 75.37°. The strongest characteristic Fe–O peaks were observed at 2-theta angles of 31.87°, 35.68°, 45.55°, 57.47° and 63.15°. From this point of view, the XRD pattern of the synthesized Fe_3O_4 was found to match the reference magnetite Fe_3O_4 pattern (JCPDS card number 19-0629), and the structure was confirmed. After the analysis of the final product, the characteristic XRD spectra of

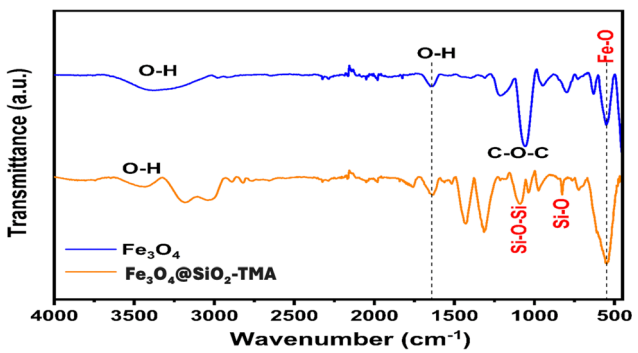

Fig. 3 FTIR spectra of the Fe_3O_4 and Fe_3O_4@SiO_2–TMA nanoparticles.

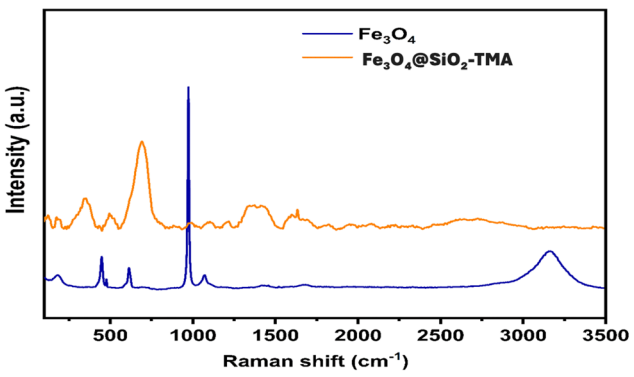

Fig. 4 Raman spectra of the Fe_3O_4 and Fe_3O_4@SiO_2–TMA nanoparticles.

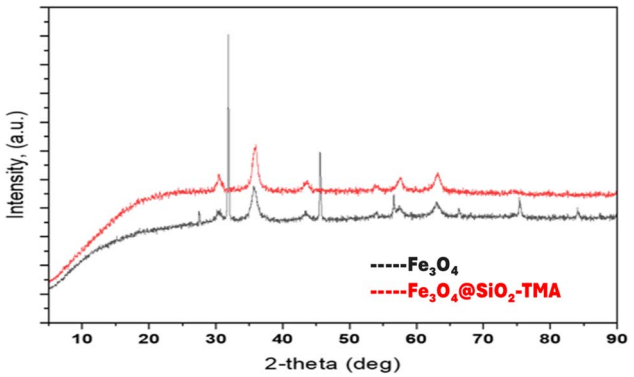

Fig. 5 XRD spectra of the Fe_3O_4 and Fe_3O_4@SiO_2–TMA nanoparticles.

the Fe_3O_4 nanomaterial were seen in the structure. In addition to these characteristic peaks, new peaks originating from SiO_2 and TMA were obtained at 2-theta angles of 30.57°, 36.04°, 43.57°, 53.92°, 57.51° and 63.15°. SiO_2 structurally behaved like an amorphous material in the XRD spectra.

The functionalization of Fe_3O_4@SiO_2 with trimesic acid was mainly attributed to interactions between the surface silanol (Si–OH) groups and the carboxylic acid functionalities of TMA. Hydrogen bonding and possible coordination interactions facilitated the immobilization of TMA onto the silica shell. The presence of aromatic rings and multiple carboxyl groups introduced additional π–π interaction and hydrogen bonding sites, which enhanced the adsorption affinity toward the azole antifungal drugs. These surface modifications were consistent with the FTIR band shifts and Raman spectral features observed after functionalization.

3.2 Optimization of the MSPE parameters

In the extraction of BFZ and IFZ target analytes utilizing Fe_3O_4@SiO_2–TMA magnetic nanomaterial, the parameters of the MSPE method were optimized to enhance extraction efficiency, improve analytical sensitivity, minimize matrix interferences, and ensure the reproducibility of the results. These optimization steps encompassed several critical parameters, including the selection of the optimal pH of the extraction process, the choice of back extraction solution and its volume, the determination of the adsorption solution along with its volume, and the duration of vortex mixing. The interaction between the analytes and the magnetic nanocomposite was enhanced by each of these factors, which played a crucial role in maximizing the efficiency and effectiveness of the extraction process. The selected sorbent amount (50 mg) was determined based on preliminary extraction trials and literature precedents for magnetic MSPE applications, providing quantitative recovery and efficient magnetic handling. The procedure involved preparing samples with MSPE and then analyzing the results with HPLC-DAD.

3.2.1 Effect of pH on MSPE. pH has the potential to influence the ionization state of the analytes and functional groups on the adsorbent. Thus, the adsorbent and analytes exhibit different solubilities and interactions. The pK_a values of specific compounds can determine the enhancement or inhibition of the extraction of specific compounds under acidic or basic conditions. The pK_a for BFZ was 6.36 with a log P of 4.92–5.23, while that of ITZ was 3.91 with a log P of 5.48–7.31. The ideal medium for optimum interactions between the analyte and the adsorbent was produced using pH. Therefore, using buffered model solutions, the MSPE technique was applied to study the influence of sample solution pH on BFZ and ITZ adsorption efficiency in the range of 2.0–10.0. The outcomes are displayed in Fig. 6. It was evident that the alkaline pH 8.0 environment helped to raise the extraction efficiency of BFZ and ITZ. The rate of extraction rises when the solution pH shifts from the acidic to the basic area. The reduction in recoveries resulting from electrostatic repulsion is related to the ease with which both molecules may carry a positive charge through protonation in an acidic medium. However, BFZ and ITZ were readily hydrolyzed in an alkaline medium, when the pH was higher than 8. Therefore, pH 8 was chosen for the next tests.

3.2.2 Selection of desorption (back extraction) eluent. The selection of desorption eluent and volume in the extraction process is directly related to the parameters such as extraction efficiency, the recovery rate of the target analyte, and preconcentration factor. The solvents that were used include methanol, ethanol, acetonitrile, water, acetonitrile: methanol (1 : 1, v/v), *n*-hexane, acetone, pH 8.0 buffer, and 2-propanol. The volume of the desorption solvent was consistently 1000 μL. The findings presented in Fig. 7 indicate that the use of water, acetone, and buffer solution did not result in successful recovery, as they were unable to effectively break the bond between the target molecules and the Fe_3O_4@SiO_2–TMA magnetic nanoparticles. As a result, the highest recoveries for the targeted BFZ and ITZ were achieved using ethanol, likely due to its strong compatibility and robust hydrogen bond and dipole–dipole interactions with our molecules. Therefore, ethanol was chosen as the eluent for the subsequent stages of this study.

The volume of solvent used to desorb the target analytes from the magnetic nanoparticles is a critical parameter that directly affects the efficiency of the enrichment process. The chosen eluent volume must be compatible with subsequent HPLC-DAD analysis. Following preliminary optimization, the enrichment procedure was tested with different volumes of

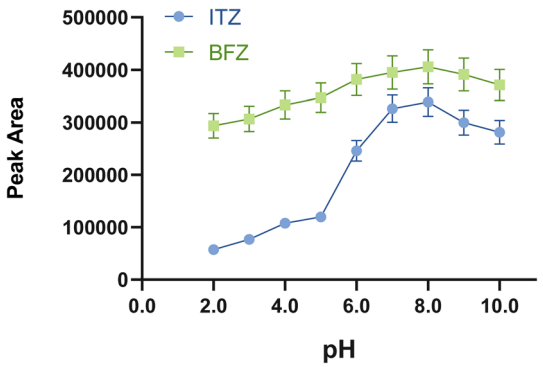

Fig. 6 Effect of pH on the MSPE of the BFZ and ITZ molecules (n:3).

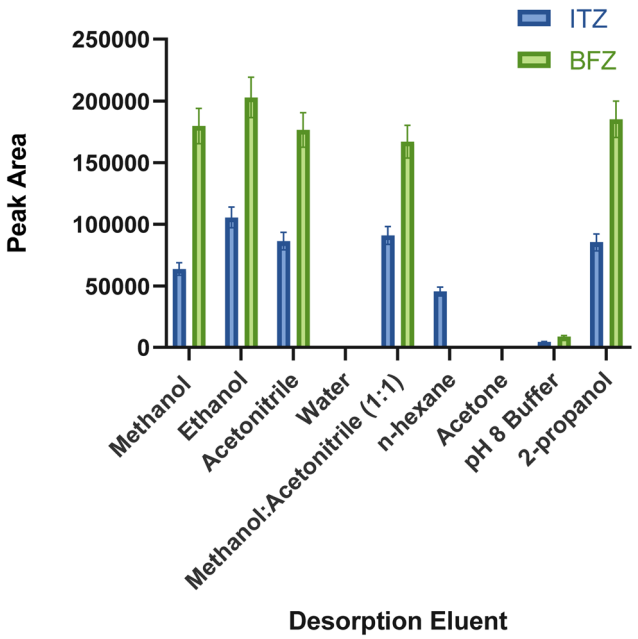

Fig. 7 Effect of various eluents on the efficient desorption of BFZ and ITZ (n:3).

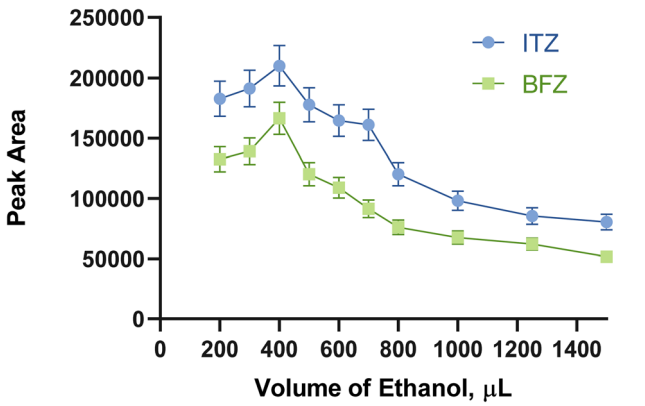

Fig. 8 Effect of ethanol volume upon the analyte responses (n:3).

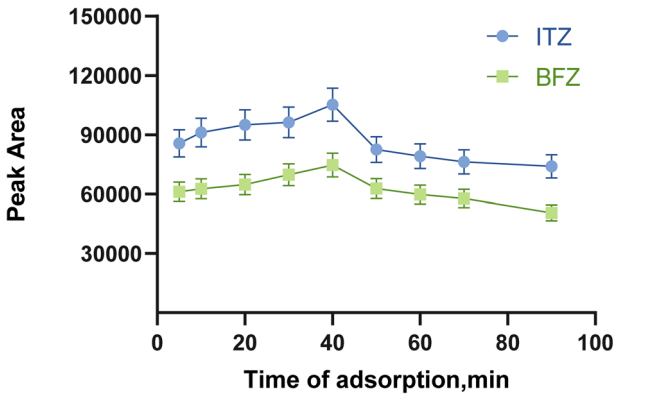

Fig. 9 Effect of adsorption time on MPSE for BFZ and ITZ (n:3).

ethanol, ranging from 200 to 1500 μL, to identify the conditions yielding the most favorable chromatographic peaks. As shown in Fig. 8, the highest peak intensity was achieved using 400 μL of ethanol. Low eluent volumes provided high preconcentration factors, whereas high volumes reduced the preconcentration efficiency due to dilution, despite effectively releasing the analytes from the nanoparticles. Because the preconcentration factor was inversely proportional to the eluent volume, 400 μL was established as the optimal volume for desorption.

3.2.3 Effect of adsorption time. The duration of the extraction process can influence the effectiveness of MSPE. If the extraction time is too short, the adsorption may not be sufficient, whereas if it is too long, there may be unnecessary losses. To assess the impact of extraction time, an orbital shaker was used at a speed of 50 rpm for a duration ranging from 5 to 90 minutes. The results, depicted in Fig. 9, indicated that the recovery of BFZ and ITZ gradually increased as the shaking time progressed from 5 to 40 minutes. However, after 40 minutes, the recovery of the target molecules began to decrease, suggesting that the adsorption equilibrium had been reached, and the process was complete. Consequently, a 40-minute extraction time was adopted for all subsequent stages of the MSPE procedure in this study.

3.2.4 Reusability and carry-over of the Fe_3O_4@SiO_2–TMA nanoparticles. The sustainable use and enrichment factor of nanoparticles largely depend on their ability to be reused repeatedly. To assess the regeneration performance of the Fe_3O_4@SiO_2–TMA nanoparticles, recycling experiments were conducted using a standardized procedure. Fig. 10 presents the results of the adsorption experiments for the 5th regeneration cycle. After each cycle, the used adsorbent was washed with a mixture of acetonitrile and methanol, then reused for the next cycle. The experimental findings demonstrated that the adsorption performance of the nanoparticles remained consistent throughout the 5 cycles, indicating the stability and reusability of the sorbent for the detection of the BFZ and ITZ molecules. Furthermore, the results suggested that the used nanoparticles exhibited excellent chemical stability for the adsorption of antifungals. To evaluate the practical reusability of the adsorbent, consecutive adsorption–desorption cycles were performed under optimum conditions. The recovery percentages of BFZ and ITZ were calculated after each cycle. The results demonstrated that the adsorbent maintained high extraction efficiency with only a slight decrease after repeated use, indicating satisfactory physicochemical stability.

The carry-over effect of the MSPE was also evaluated by measuring the residual amount of analytes after each use. To conduct this evaluation, 5 model solutions containing drug molecules were prepared and subjected to the developed MSPE method. The efficacy of the magnetic nanoparticles in desorbing molecules from the first application was demonstrated by the fact that nearly 75% of BFZ and ITZ were detected in the initial desorption, as illustrated in Fig. 11. This results indicate that the efficacity of the synthesized magnetic nanoparticles to desorb the molecules from the first application.

3.2.5 Analytical performance. Using the optimum extraction conditions, the performance of the MSPE-HPLC-DAD methodology was evaluated by calculating the linearity,

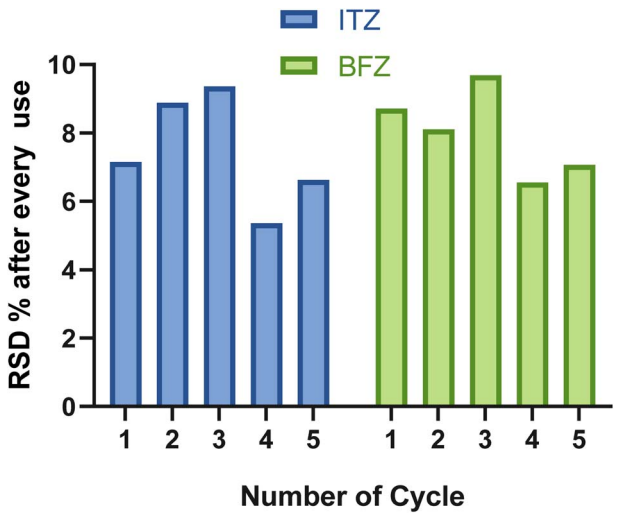

Fig. 10 Reusability of the Fe_3O_4@SiO_2–TMA nanoparticles over 5 cycles.

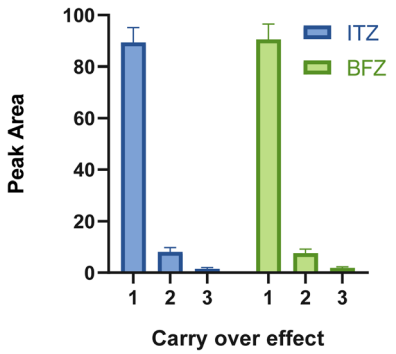

Fig. 11 Carry-over effect of the Fe_3O_4@SiO_2–TMA nanoparticles.

correlation coefficient, limit of detection (LOD), limit of quantification (LOQ), enhancement factor (EF), preconcentration factor (PF) and relative standard deviation (RSD%), which are reported in Table 2. After applying the proposed method, the linear range was improved from 1.00–20.00 μg mL^{-1} to 15.00–1000.00 ng mL^{-1} for both molecules with a correlation coefficient (R^2) ≥ 0.9950.

The limits of detection (LOD) and quantification (LOQ) were evaluated in accordance with ICH Q2(R1) guidelines. Calibration curves were constructed using concentration levels close to the estimated detection and quantification ranges. The residual standard deviation of the regression line (root mean square deviation) and the standard deviation of the *y*-intercepts of the calibration plots were considered as statistical parameters. LOD and LOQ were estimated using the expressions LOD = $3.3\sigma/S$ and LOQ = $10\sigma/S$, where σ represents the standard deviation of the response, and S is the slope of the calibration curve.

The limit of detection (LOD) and limit of quantification (LOQ) were defined based on signal-to-noise ratio (S/N) of 3 and 10, respectively.[39,40] Preconcentration factors (PF) were calculated using the ratio of the initial solution volume (50 mL) to the optimum elution solvent volume (400 μL). Moreover, the enhancement factor (EF) of the MSPE method was described as the ratio between the slope of the calibration curve obtained after pre-concentration and the slope of the calibration curve prior to pre-concentration. The experiments revealed that the RSD of target molecules ranged from 2.7% to 6.5%, indicating the good precision and stability of the developed method.

3.2.6 Application of MSPE-HPLC-DAD on urine, saliva and pharmaceutical samples. In order to show the correctness and the applicability of this methodology, urine, saliva and pharmaceutical samples were used to determine the amount of fungicides under the optimum parameters using MSPE application. Using different concentrations of standards, recovery and RSD% values were successfully calculated in each solution, and the results are depicted in Table 3. However, the recovery values were between 94.7% and 107.5%, and the RSD% varied between 2.7% and 7.3%. According to the obtained data, it could be proved that the developed MSPE-HPLC-DAD process was accurate and precise for the extraction of BFZ and ITZ.

3.3 Evaluation of blue applicability grade index (BAGI) for the developed method

The performance and applicability of the developed analytical method were systematically assessed using two complementary evaluation tools: the Blue Applicability Grade Index (BAGI) and the Model-based Green Analytical Procedure Index (MoGAPI). BAGI, introduced by Manousi *et al.*,[41,42] offers a contemporary

Table 2 Analytical properties of the developed MSPE-based HPLC analysis method

	Without MSPE		With MSPE	
Parameter	ITZ	BFZ	ITZ	BFZ
Linear range	1.00–20.00 μg mL^{-1}	1.00–20.00 μg mL^{-1}	15.00–1000.00 ng mL^{-1}	15.00–1000.00 ng mL^{-1}
LOD	0.32 μg mL^{-1}	0.36 μg mL^{-1}	4.54 ng mL^{-1}	4.78 ng mL^{-1}
LOQ	0.95 μg mL^{-1}	0.90 μg mL^{-1}	14.14 ng mL^{-1}	14.50 ng mL^{-1}
Calibration sensitivity	14.29	7.96	1886.3	939.3
R^2	0.9977	0.9947	0.9954	0.9970
Preconcentration factor[a]	—	—	125	125
Enhancement factor[b]	—	—	132	118

[a] Preconcentration factor is defined as the ratio of the initial solution volume (50 mL) to the final volume of solution (400 μL). [b] Enhancement factor is defined as the ratio of the slope of calibration before and after MPSE.

Table 3 Results of sample analysis using the developed MSPE-based HPLC

Samples	Added (ng mL^{-1})	Found[a] (ng mL^{-1})		RSD (%)		Recovery (%)	
		ITR	BFZ	ITR	BFZ	ITR	BFZ
Artificial urine	0.0	<LOD	<LOD	—	—	—	—
	250.0	236.8 ± 12.4	246.5 ± 9.1	5.2	3.7	94.7	98.6
	500.0	496.5 ± 23.8	512.5 ± 23.4	4.8	4.6	99.3	102.5
Artificial saliva	0.0	<LOD	<LOD	—	—	—	—
	250.0	264.5 ± 11.4	240.8 ± 10.7	4.3	4.4	105.8	95.9
	500.0	504.5 ± 13.6	483.2 ± 27.1	2.7	5.6	100.9	95.7
Pharmaceutical samples	0.0	75.8 ± 4.8	124.5 ± 7.8	6.3	6.3	—	—
	250.0	312.4 ± 18.7	402.5 ± 24.5	6.0	6.1	95.9	107.5
	500.0	550.8 ± 26.7	642.5 ± 41.7	4.8	6.5	95.7	102.9

[a] Mean ± standard deviation.

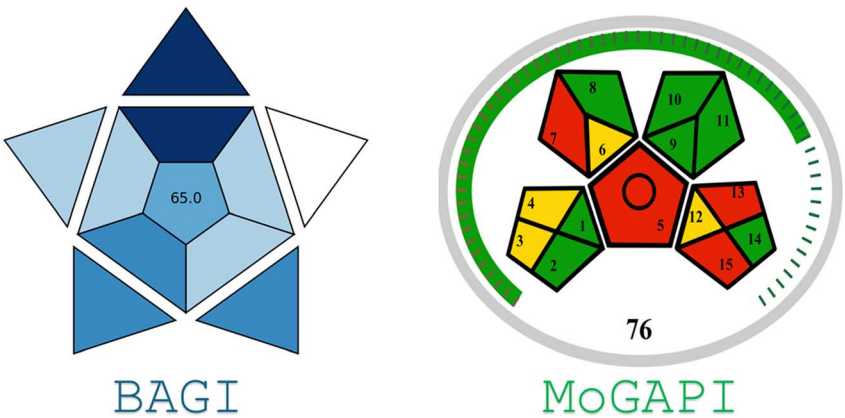

Fig. 12 BAGI and MOGAPI evaluation of the developed method.

framework that expands upon traditional green assessment approaches by emphasizing operational feasibility within the principles of white analytical chemistry. It incorporates ten practical criteria—including analytical format, number of analytes, instrumentation, sample preparation, parallel sample handling, hourly throughput, reagent type, preconcentration requirements, automation level, and sample consumption—to produce a score between 25 and 100, with values ≥60 indicating acceptable applicability. The method obtained a BAGI score of 65, demonstrating satisfactory practicality and efficient workflow characteristics.

In parallel, the score of 76 reflected the method's strong structural integrity and consistency with green analytical principles.[43] This value indicated an appropriate balance between model reliability, parameter stability, and predictive suitability across the study domains. The score suggested that the procedure provided environmentally conscious choices in reagents, energy use, and waste generation while retaining analytical

Table 4 Comparative assessment of the literature-reported and proposed analytical methods for BFZ and ITZ determination with respect to detection limits, extraction approaches, recovery, and practical applicability

Method	Analyte	Matrix	LOD	Recovery (%)	Pretreatment	Ref.
HPLC-UV	ITZ	Human plasma	5.0 ng mL^{-1}	89.1–98.2	SPE	44
HPLC-PDA	ITZ	Human serum	60 ng mL^{-1}	97.3–103.9	LLE	45
HPLC-FLD	ITZ	Plasma/tissue	151 ng mL^{-1}	83–106	Protein precipitation	46
UV-vis spectrophotometry	ITZ	Pharmaceutical dosage form	1580 ng mL^{-1}	No data	Dilution	47
LCMS/MS	ITZ	Human plasma	20 ng mL^{-1}	90.0–110.0	Dilution	48
HPLC-DAD	ITZ, BFZ	Biological samples	17 ng mL^{-1}	90–96	Microextraction by packed sorbent	49
HPLC-PDA	ITZ, BFZ	Human plasma and urine	30 ng mL^{-1}	91–97	Fabric phase sorptive extraction (FPSE)	50
HPLC-DAD	BFZ, ITZ	Urine/saliva	5 ng mL^{-1}	94–102	MSPE	This work

robustness. Together, the BAGI and MoGAPI evaluations confirmed that the proposed method was both operationally feasible and aligned with modern sustainability and quality expectations, offering a solid basis for further refinement and broad analytical application. BAGI and MoPAPI pictograms of the developed method are shown in Fig. 12.

4. Conclusion

The trace determination of drug molecules is important to monitor their toxicological and therapeutic effects. Moreover, a lot of chemical analyses are performed in drug development projects. So, new analytical methods receive great attention as alternatives to existing ones.

The performance of the developed Fe_3O_4@SiO_2–TMA adsorbent was evaluated in comparison with previously reported MSPE sorbents used for antifungal drug extraction. The proposed material provided several advantages, including rapid magnetic phase separation, high extraction efficiency, and improved selectivity due to π–π interactions and hydrogen bonding between the trimesic acid moieties and analyte structures. Moreover, the sorbent required low material consumption and short extraction time, contributing to its operational simplicity and cost-effectiveness when applied to complex biological matrices.

The analytical performance of the proposed MSPE-HPLC method was compared with those of reported methods for the determination of BFZ and ITZ. As summarized in Table 4, the developed approach provided competitive or relatively low detection limits, satisfactory recovery values, and short pretreatment times. In addition, magnetic separation capability, sorbent reusability, and favorable greenness scores offered practical advantages over conventional extraction techniques.

The proposed methodology presented a simple approach for the sensitive and simultaneous determination of bifonazole and itraconazole drug molecules. A new magnetic material, Fe_3O_4@SiO_2–TMA, was synthesized and characterized to collect target molecules from samples. The reusability of Fe_3O_4@SiO_2–TMA was shown with recovery and carry-over tests.

Author contributions

AA: investigation and formal analysis; HİU: data curation and writing – original draft; ÜP: validation and data curation; SU: writing – review and editing and conceptualization; and HK: data curation.

Conflicts of interest

The authors declare that they have no known competing financial interests or personal relationships that could have appeared to influence the work reported in this paper.

Data availability

The data supporting the findings of this study are available from the corresponding author upon reasonable request.

Acknowledgements

This work was kindly supported by the Sivas Cumhuriyet University Scientific Research Projects Commission (CUBAP) under project number ECZ-2023-093. The authors also sincerely thank Dr Gökhan Sarp for his valuable assistance in the characterization of the magnetic particles.

References

1 G. Wall and J. L. Lopez-Ribot, Current antimycotics, new prospects, and future approaches to antifungal therapy, *Antibiotics*, 2020, **9**(8), 445.
2 M. Roy, S. Karhana, M. Shamsuzzaman and M. A. Khan, Recent drug development and treatments for fungal infections, *Braz. J. Microbiol.*, 2023, **54**, 1695–1716.
3 M. Zavrel, B. D. Esquivel and T. C. White, in *Handbook of Antimicrobial Resistance*, Springer New York, New York, NY, 2017, pp. 423–452.
4 G. D'Orazio, C. Fanali, C. Dal Bosco, A. Gentili and S. Fanali, Chiral separation and analysis of antifungal drugs by chromatographic and electromigration techniques: results achieved in 2010–2020, *Rev. Anal. Chem.*, 2021, **40**, 220–252.
5 M. A. Mohamed, N. N. Salama, M. A. Sultan, H. F. Manie and M. M. A. El-Alamin, Sensitive and effective electrochemical determination of butenafine in the presence of itraconazole using titanium nanoparticles-ionic liquid based nanocomposite sensor., *Chem. Pap.*, 2023, **77**, 1929–1939.
6 F. Almeida-Silva, D. de Souza Gonçalves, M. de Abreu Almeida and A. J. Guimarães, Current aspects of diagnosis and therapeutics of histoplasmosis and future trends: moving onto a new immune (diagnosis and therapeutic) era?, *Curr. Clin. Microbiol. Rep.*, 2019, **6**, 98–107.
7 S. Yang, D. Yan, M. Li, D. Li, S. Zhang, G. Fan, L. Peng and S. Pan, Ergosterol depletion under bifonazole treatment induces cell membrane damage and triggers a ROS-mediated mitochondrial apoptosis in Penicillium expansum, *Fungal Biol.*, 2022, **126**, 1–10.
8 A. M. Burden, L. Hausammann, A. Ceschi, H. Kupferschmidt and S. Weiler, Observational cross-sectional case study of toxicities of antifungal drugs, *J. Global Antimicrob. Resist.*, 2022, **29**, 520–526.
9 Z. Cheng, J. Liang, Y. Hu, Q. Lv, X. Li and X. Shen, Comprehensive evaluation of solvent in dispersive liquid-liquid microextraction for determination of itraconazole and hydroxy itraconazole by high performance liquid chromatography with fluorescence detection, *Arabian J. Chem.*, 2023, **16**, 104565.
10 N. Othman, V. Lim, M. R. Ramachandran, M. M. Sanagi, S. Kamaruzaman, Y. Hirota, N. Nishiyama and N. Yahaya, Rapid ultrasound-assisted emulsification microextraction

combined with COU-2 dispersive micro-solid phase extraction for the determination of azole antifungals in milk samples by HPLC-DAD, *Chromatographia*, 2017, **80**, 1553–1562.

11 B. Ebrahimpour, Y. Yamini and A. Esrafili, Extraction of azole antifungal drugs from milk and biological fluids using a new hollow fiber liquid-phase microextraction and analysis by GC-FID, *Chromatographia*, 2011, **74**, 281–289.

12 M.-C. Jäger, F. L. Joos, D. V. Winter and A. Odermatt, Characterization of the interferences of systemic azole antifungal drugs with adrenal steroid biosynthesis using H295R cells and enzyme activity assays, *Curr. Res. Toxicol.*, 2023, **5**, 100119.

13 Y. Yu, J. Zhang, B. Shao, Y. Wu, H. Duan and H. Liu, Development of a simple liquid chromatography-tandem mass spectrometry method for multiresidue determination of antifungal drugs in chicken tissues, *J. AOAC Int.*, 2011, **94**, 1650–1658.

14 R. J. Ekiert, J. Krzek and W. Rzeszutko, Evaluation of a TLC densitometric method for analysis of azole antifungal agents, *Chromatographia*, 2008, **67**, 995–998.

15 C. Campestre, M. Locatelli, P. Guglielmi, E. De Luca, G. Bellagamba, S. Menta, G. Zengin, C. Celia, L. Di Marzio and S. Carradori, Analysis of imidazoles and triazoles in biological samples after MicroExtraction by packed sorbent., *J. Enzyme Inhib. Med. Chem.*, 2017, **32**, 1053–1063.

16 N. Manousi, A. Vlachaki, F. S. Kika, C. K. Markopoulou, P. D. Tzanavaras and C. K. Zacharis, Salting-out homogeneous liquid-liquid microextraction for the determination of azole drugs in human urine: validation using total error concept, *J. Sep. Sci.*, 2022, **45**, 1240–1251.

17 K. Bashir, G. Chen, J. Han, H. Shu, X. Cui, L. Wang, W. Li and Q. Fu, Preparation of magnetic metal organic framework and development of solid phase extraction method for simultaneous determination of fluconazole and voriconazole in rat plasma samples by HPLC, *J. Chromatogr. B*, 2020, **1152**, 122201.

18 N. Othman, V. Lim, M. R. Ramachandran, M. M. Sanagi, S. Kamaruzaman, Y. Hirota, N. Nishiyama and N. Yahaya, Rapid ultrasound-assisted emulsification microextraction combined with COU-2 dispersive micro-solid phase extraction for the determination of azole antifungals in milk samples by HPLC-DAD, *Chromatographia*, 2017, **80**, 1553–1562.

19 T. Tuominen, D. Perera, G. Russo and S. K. Wiedmer, Liquid Chromatographic and Capillary Electromigration Techniques for the Analysis of Azole Antifungals, *J. Sep. Sci.*, 2025, **48**, e70135.

20 E. Durgun, H. İ. Ulusoy and İ. Narin, Sensitive, reliable and simultaneous determination of Fingolimod and Citalopram drug molecules used in multiple sclerosis treatment based on magnetic solid phase extraction and HPLC-PDA, *J. Chromatogr. B: Anal. Technol. Biomed. Life Sci.*, 2024, 124071.

21 X. Zhang, H. Xu, C. Zhou, L. Yang, S. Zhai, P. Yang, R. Zhao and R. Li, Magnetic solid phase extraction followed by in-situ derivatization with core–shell structured magnetic graphene oxide nanocomposite for the accurate quantification of free testosterone and free androstenedione in human serum, *J. Chromatogr. B*, 2022, **1196**, 123188.

22 H.-L. Jiang, Q.-B. Fu, M.-L. Wang, J.-M. Lin and R.-S. Zhao, Determination of trace bisphenols in functional beverages through the magnetic solid-phase extraction with MOF-COF composite, *Food Chem.*, 2021, **345**, 128841.

23 A. L. Capriotti, C. Cavaliere, G. La Barbera, C. M. Montone, S. Piovesana and A. Laganà, Recent applications of magnetic solid-phase extraction for sample preparation, *Chromatographia*, 2019, **82**, 1251–1274, DOI: 10.1007/s10337-019-03721-0.

24 K. Chinchan, S. Jiajaroen, C. Theppitak, S. Laksee, M. Sukwattanasinitt and K. Chainok, Synthesis, structure and photoluminescence properties of heterometallic-based coordination polymers of trimesic acid, *Acta Crystallogr., Sect. C: Struct. Chem.*, 2024, **80**, 230–238.

25 S. Moorthy, B. Maria Mahimai, D. Kannaiyan and P. Deivanayagam, Synthesis and fabrication of Cu-trimesic acid MOF anchored sulfonated Poly (2, 5-benzimidazole) membranes for PEMFC applications, *Int. J. Hydrogen Energy*, 2023, **48**, 36063–36075.

26 Z. Mirzaei Karazan, M. Roushani and S. Jafar Hoseini, Simultaneous electrochemical sensing of heavy metal ions (Zn2+, Cd2+, Pb2+, and Hg2+) in food samples using a covalent organic framework/carbon black modified glassy carbon electrode, *Food Chem.*, 2024, **442**, 138500.

27 S.-L. Zhang, L. Yu, P.-C. Su, H.-W. Ge, M.-T. Sun and S.-H. Wang, Microwave synthesis of zinc-trimesic acid metal–organic framework for visual fluorescence detection of tetracyclines., *Chem. Pap.*, 2022, **76**, 4777–4786.

28 A. Khalid, R. M. Ahmed, M. Taha and T. S. Soliman, Fe3O4 nanoparticles and Fe3O4@ SiO2 core-shell: synthesize, structural, morphological, linear, and nonlinear optical properties., *J. Alloys Compd.*, 2023, **947**, 169639.

29 J. Hou, C. Hu, H. Li, H. Liu, Y. Xiang, G. Wu and Y. Li, Nanomaterial-based magnetic solid-phase extraction in pharmaceutical and biomedical analysis, *J. Pharm. Biomed. Anal.*, 2025, **253**, 116543.

30 H. I. Ulusoy, U. Polat and S. Ulusoy, Use of newly synthetized magnetic Fe 3 O 4 nanoparticles modified with hexadecyl trimethyl ammonium bromide for the sensitive analysis of antidepressant drugs, duloxetine and vilazodone in wastewater and urine samples, *RSC Adv.*, 2023, **13**, 20125–20134.

31 H. İ. Ulusoy, *Applications of Magnetic Nanoparticles for the Selective Extraction of Trace Species from a Complex Matrix*, Nova Scientific Publishers, New York, 1st edn, 2017.

32 M. Sarıkaya, H. I. Ulusoy, U. Morgul, S. Ulusoy, A. Tartaglia, E. Yılmaz, M. Soylak, M. Locatelli and A. Kabir, Sensitive determination of Fluoxetine and Citalopram antidepressants in urine and wastewater samples by liquid chromatography coupled with photodiode array detector., *J. Chromatogr. A*, 2021, 462215.

33 Ş. Temiz, S. Ulusoy, H. İ. Ulusoy, E. Durgun, Ü. Polat and G. Sarp, Synthesis and use of new magnetic adsorbent for sensitive, practical and simultaneous analysis Ibuprofen

and Ketoprofen molecules in urine samples, *J. Chromatogr. B: Anal. Technol. Biomed. Life Sci.*, 2025, 124404.

34 N. Sarigul, F. Korkmaz and İ. Kurultak, A new artificial urine protocol to better imitate human urine, *Sci. Rep.*, 2019, **9**, 1–11.

35 E. E. Herbei, D. L. Buruiana, A. C. Muresan, V. Ghisman, N. L. Bogatu, V. Basliu, C.-I. Vasile and L. Barbu-Tudoran, Tailored Magnetic Fe3O4-Based Core–Shell Nanoparticles Coated with TiO2 and SiO2 via Co-Precipitation: Structure–Property Correlation for Medical Imaging Applications, *Diagnostics*, 2025, **15**, 1912.

36 S. Khashan, S. Dagher, S. Al Omari, N. Tit, E. Elnajjar, B. Mathew and A. Hilal-Alnaqbi, Photo-thermal characteristics of water-based Fe3O4@ SiO2 nanofluid for solar-thermal applications, *Mater. Res. Express*, 2017, **4**, 055701.

37 D. Y. Medina-Velazquez, B. Y. Alejandre-Zuniga, S. Loera-Serna, E. M. Ortiz, A. de Jesus Morales-Ramirez, E. Garfias-Garcia, A. Garcia-Murillo and C. Falcony, An alkaline one-pot reaction to synthesize luminescent Eu-BTC MOF nanorods, highly pure and water-insoluble, under room conditions., *J. Nanopart. Res.*, 2016, **18**, 352.

38 O. N. Shebanova and P. Lazor, Raman spectroscopic study of magnetite (FeFe2O4): a new assignment for the vibrational spectrum, *J. Solid State Chem.*, 2003, **174**, 424–430.

39 ICH, alidation of Analytical Procedures: Text and Methodology Q2(R1), International Council for Harmonisation, 2005.

40 D. Kumar, G. Singh and D. Bairagee, Chromatographic Method Development and Validation Assay of Apremilast in Tablet Dosage Form, *Int. J. Pharm. Life Sci.*, 2020, **11**(9), 6989–6994.

41 F. Pena-Pereira, W. Wojnowski and M. Tobiszewski, Analytical GREEnness metric approach and software., *Anal. Chem.*, 2020, **92**, 10076–10082.

42 N. Manousi, J. Płotka-Wasylka and V. Samanidou, Novel sorptive extraction techniques in bioanalysis evaluated by Blue Applicability Grade Index: the paradigm of fabric phase sorptive extraction and capsule phase microextraction, *TrAC, Trends Anal. Chem.*, 2024, 117586.

43 F. R. Mansour, J. Płotka-Wasylka and M. Locatelli, Modified GAPI (MoGAPI) tool and software for the assessment of method greenness: case studies and applications, *Analytica*, 2024, **5**, 451–457.

44 T. Ohkubo and T. Osanai, Determination of itraconazole in human plasma by high-performance liquid chromatography with solid-phase extraction, *Ann. Clin. Biochem. Int. J. Lab. Med.*, 2005, **42**(2), 94–98.

45 E. Cendejas-Bueno, M. Cuenca-Estrella and A. Gomez-Lopez, A simple, sensitive HPLC-PDA method for the quantification of itraconazole and hydroxy itraconazole in human serum: a reference laboratory experience, *Diagn. Microbiol. Infect. Dis.*, 2013, **76**, 314–320.

46 K. R. Py-Daniel, O. R. Pires Junior, C. M. I. Cordova, M. L. Fascineli, A. C. Tedesco and R. B. Azevedo, HPLC-FLD method for itraconazole quantification in poly lactic-co-glycolic acid nanoparticles, plasma and tissue, *J. Braz. Chem. Soc.*, 2014, **25**(4), 697–703.

47 L. A. G. Pinho, L. C. L. Sá-Barreto, C. M. C. Infante and M. S. S. Cunha-Filho, Simultaneous determination of benznidazole and itraconazole using spectrophotometry applied to the analysis of mixture: a tool for quality control in the development of formulations, *Spectrochim. Acta, Part A*, 2016, **159**, 48–52.

48 N. Jenkins, M. Black and H. G. Schneider, Simultaneous determination of voriconazole, posaconazole, itraconazole and hydroxy-itraconazole in human plasma using LCMS/MS, *Clin. Biochem.*, 2018, **53**, 110–115.

49 C. Campestre, M. Locatelli, P. Guglielmi, E. De Luca, G. Bellagamba, S. Menta, G. Zengin, C. Celia, L. Di Marzio and S. Carradori, Analysis of imidazoles and triazoles in biological samples after MicroExtraction by packed sorbent, *J. Enzyme Inhib. Med. Chem.*, 2017, **32**, 1053–1063.

50 M. Locatelli, A. Kabir, D. Innosa, T. Lopatriello and K. G. Furton, A fabric phase sorptive extraction-high performance liquid chromatography-photo diode array detection method for the determination of twelve azole antimicrobial drug residues in human plasma and urine, *J. Chromatogr. B*, 2017, **1040**, 192–198.